PHYSICAL REVIEW MATERIALS **2**, 011601(R) (2018)

Rapid Communications   Editors' Suggestion

Elastically frustrated rehybridization: Origin of chemical order and compositional limits in InGaN quantum wells

L. Lymperakis,[1,*] T. Schulz,[2,†] C. Freysoldt,[1] M. Anikeeva,[2] Z. Chen,[3] X. Zheng,[3] B. Shen,[3] C. Chèze,[4] M. Siekacz,[5] X. Q. Wang,[3,6,‡] M. Albrecht,[2] and J. Neugebauer[1]

[1]*Max-Planck-Institut für Eisenforschung GmbH, Max-Planck-Straße 1, 40237 Düsseldorf, Germany*

[2]*Leibniz-Institute for Crystal Growth, Max-Born-Straße 2, 12489 Berlin, Germany*

[3]*State Key Laboratory of Artificial Microstructure and Mesoscopic Physics, School of Physics, Peking University, Beijing 100871, China*

[4]*Paul Drude Institute für Festkörperelektronik, Hausvogteiplatz 5-7, 10117, Berlin, Germany*

[5]*Institute of High Pressure Physics, Polish Academy of Sciences, Sokolowska 29/37, 01-142 Warsaw, Poland*

[6]*Collaborative Innovation Center of Quantum Matter, Beijing, China*

(Received 16 May 2017; revised manuscript received 14 July 2017; published 8 January 2018)

Nominal InN monolayers grown by molecular beam epitaxy on GaN(0001) are investigated combining *in situ* reflection high-energy electron diffraction (RHEED), transmission electron microscopy (TEM), and density functional theory (DFT). TEM reveals a chemical intraplane ordering never observed before. Employing DFT, we identify a novel surface stabilization mechanism elastically frustrated rehybridization, which is responsible for the observed chemical ordering. The mechanism also sets an incorporation barrier for indium concentrations above 25% and thus fundamentally limits the indium content in coherently strained layers.

DOI: 10.1103/PhysRevMaterials.2.011601

Modern optoelectronic devices rely on our ability to tune the electronic band structure of ultrathin heteroepitaxial structures via the chemical composition [1–3]. A prime challenge often encountered when designing and optimizing such devices is the failure to achieve the targeted chemical composition. This is related to the fact that the specific composition is thermodynamically or kinetically unstable. $In_xGa_{1-x}N$ alloys are a prime example where such thermodynamic limitations have a severe impact on device features and performances. If the In composition in these alloys could be controlled from $x = 0$ (GaN; band gap 3.5 eV) all the way up to $x = 1$ (InN; band gap 0.7 eV), light emitting devices from the infrared to the ultraviolet region could be realized. However, so far, the uppermost In concentrations in coherently grown 2D (In,Ga)N layers were reported to be around 30% [4–6], which severely narrows the tunability of InGaN-based emitters.

Such stoichiometric limits may be overcome if the thermodynamic stability for a given composition is more favourable at the surface than in bulk. In coherently grown heteroepitaxial layers, the loss of translation symmetry at the growth surface as well as the strain introduced by the lattice mismatch may shift the thermodynamic potential of the system, stabilizing alloys that are unstable in the bulk state [7–11]. Important phenomena related to this mechanism are compositional latching [12,13], strain enhanced solubility via suppression of phase separation or spinodal decomposition [14–16], or increased miscibility of compounds at the surface, which are unstable in the bulk [11,17,18]. While these aspects have been discussed in detail in the past, less attention has been paid to the effects of surface termination and surface reconstructions on thermal decomposition of the constituents and its role in controlling alloy composition or chemical ordering. Motivated by this, we have studied stoichiometric limitations in the (In,Ga)N system in samples grown by means of plasma assisted molecular beam epitaxy (PAMBE). For this purpose, we have combined *in situ* RHEED, high-resolution TEM, and *ab initio* calculations.

In this Rapid Communication, we show that deposition of a nominal InN monolayer (ML, i.e., switching off the Ga-flux) forms a chemically ordered $In_xGa_{1-x}N$ ML, exhibiting a mean In content of 25%, even a systematic wide-range variation of the growth parameters did not succeed in overcoming this compositional limit. Employing DFT calculations in combination with thermodynamic concepts we show that a novel surface mechanism—*elastically frustrated rehybridization*—leads to surface geometries that defy our present understanding of surface stabilizing mechanisms, as well as to severe stoichiometric limitations.

We targeted to grow short period superlattices consisting of InN MLs separated by GaN barriers on GaN (0001) surfaces for band gap tuning via changing the width of the barrier [19]. Using only binary compounds supposedly avoids strong local compositional inhomogeneities as present in conventional pseudobinary InGaN alloys with high indium contents [20]. After growth of a GaN buffer layer at 800 °C on a GaN (0001) template on sapphire substrate, we start the deposition of the superlattice. For this purpose, the growth temperature is reduced to 550 °C–650 °C, the Ga flux is switched off and the surface is kept under N flux to remove metallic Ga from the surface. Then the Ga shutter is closed and the In shutter is opened for depositing a ML of nominal InN on the GaN surface. Finally, the In flux is switched off and the nominal InN layer is capped by a GaN barrier. The short period superlattices typically consist of 10 periods. The GaN barriers are deposited

*Corresponding author: lymperakis@mpie.de

†Corresponding author: tobias.schulz@ikz-berlin.de

‡Corresponding author: wangshi@pku.edu.cn

    ©2018 American Physical Society

FIG. 1. (a) Experimental images of the (In,Ga)N ML region using negative Cs imaging conditions in (a) the $\langle 1\bar{1}00\rangle$ and (b) the $\langle 11\bar{2}0\rangle$ zone axis. TEM image simulations of an (In,Ga)N ML with an In content of 25% in the (c) $\langle 1\bar{1}00\rangle$ and (d) $\langle 11\bar{2}0\rangle$ zone axis. 90% of the In atoms are arranged in a $(2\sqrt{3}\times 2\sqrt{3})$R30° configuration and 10% are randomly distributed. Specimen thickness for the $\langle 1\bar{1}00\rangle$ was 7 nm; for the $\langle 11\bar{2}0\rangle$ 14 nm.

at a fixed III/V ratio of 1.1 adopting the growth temperature of the respective InN layer. Descriptions of the generic growth processes can be found in Refs. [21–24]. Structural and compositional analyses were performed in an aberration corrected transmission electron microscope (TEM) FEI Titan 80-300, operated at 300 keV and equipped with an on-axis mounted EAGLE charge coupled device (CCD) camera.

Systematically varying the growth parameters for the (In,Ga)N deposition, such as temperature (550 °C–650 °C), III/V ratio (0.8–1.5), N flux (6–14 nm/min) or growth time (4–64 s, corresponding to nominal thicknesses of 2–32 MLs of InN) neither resulted in a layer thickness exceeding a single ML nor a change in the observed composition in the TEM micrographs. Figure 1(a) displays a typical TEM image of the (In,Ga)N ML recorded in the $\langle 1\bar{1}00\rangle$ zone axis. The (In,Ga)N ML is characterized by a periodic intensity variation, with each third atomic column appearing darker than the surrounding GaN matrix. Under the imaging conditions used, these darker spots indicate atomic columns with a high In content, while the bright spots refer to atomic columns composed of GaN. The ordering occurs in patches extending several nanometers within the ML plane. In the $\langle 11\bar{2}0\rangle$ zone axis [see Fig. 1(b)], the ML is practically indistinguishable by means of contrast from the surrounding GaN matrix. While the 3× periodicity has been observed earlier by RHEED as a transient phenomenon [25], the persistence after overgrowth demonstrated by TEM (and invisible to RHEED) has to our knowledge never been observed before.

The experimentally observed 3× periodicity could be explained by recent theoretical findings according to which a $\sqrt{3}\times\sqrt{3}$ In ordered ML with a 33% In concentration is a $T = 0$ K thermodynamic ground state [26]. However, this previously identified ordered structure is not stable at our experimental growth temperatures (see Ref. [27]). We performed extensive DFT and Monte Carlo calculations for a variety of bulk and surface alloys, which will be reported elsewhere, and the key outcome was that single (In,Ga)N MLs embedded in a GaN matrix always undergo an order-disorder transition well below the actual growth temperature. We therefore conclude that the experimentally observed ordering cannot be explained by the thermodynamic stability of the embedded ordered $In_xGa_{1-x}N$ quantum well. Rather, it must be the result of an ordered surface structure, different from the In-adlayer structure studied in Ref. [26] that is stable only under In-rich growth conditions. Furthermore, it is thermodynamically stable at growth temperature and keeps stable even if overgrown by GaN.

In order to test this hypothesis, we systematically varied surface reconstruction, total In concentrations, and chemical ordering of (0001) (In,Ga)N surfaces. The surface energy of these structures were computed by DFT calculations within the local density approximation (LDA). The surfaces were modeled with a slab geometry with various surface unit cells: $(n\sqrt{3}\times n\sqrt{3})$R30° ($n = 1, 2$), $n\times n$ ($n = 1, 2, 3, 4$), as well as orthogonal $(n\times n)$R90° ($n = 2, 4$).

We first focus on surface geometries that can be rationalized by well-established principles. (1) For N-rich conditions, group-III-nitride surfaces are expected to obey the electron counting rule (ECR), i.e., all N/metal dangling bonds should be doubly occupied/empty, respectively [28,29]. This rule restricts severely the number of possible configurations. (2) For a given reconstruction, Ga/In distribution tends to maximize the number of Ga-N bonds at the expense of In-N bonds, because the latter ones have a significantly weaker bond energy. In consequence, undercoordinated sites, where the cation has not four but only three or two nitrogen neighbors, will be preferentially occupied by In since this minimizes the number of weak In-N bonds. This highly intuitive picture has been successfully used to explain various phenomena on (In,Ga)N surfaces [30,31]. (3) In atoms tend to stay away from each other to minimize dilatational stress at short distances. The stress is a consequence of the larger atomic radius of In compared to Ga, which makes the In-N bond length ≈11% longer than the Ga-N one.

It turned out that none of the energetically preferred structures constructed from these principles could explain the experimentally observed $(\sqrt{3}\times\sqrt{3})$R30° like structure or a multiple thereof. We therefore extended our search to non-conventional structures that disobey some or all of the above criteria. This search revealed that, although the ECR is valid

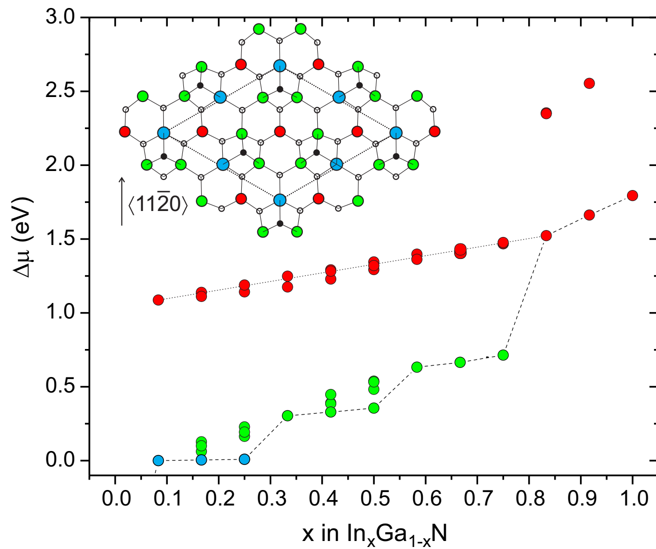

FIG. 2. Chemical potential $\Delta\mu = E^{\text{tot}}_{n+1} - E^{\text{tot}}_{n}$ as a function of composition x. E^{tot}_{n} is the total energy of a $(2\sqrt{3} \times 2\sqrt{3})\text{R}30^\circ$ slab with n In atoms in the top surface layer. Green/blue and red dots correspond to the lowest- and higher-energy configuration/s for each x, respectively. The dashed lines are guidelines for the eye. (Inset) Top view of the lowest-energy $(2\sqrt{3} \times 2\sqrt{3})\text{R}30^\circ$ $\text{In}_{0.25}\text{Ga}_{0.75}\text{N}$ configuration. Small/black dots denote the N adatoms and small/open balls the N atoms. Blues balls indicate the In atoms and red and green balls distinguish the coordination inequivalent Ga atoms. Group-III atoms at the red sites are triply coordinated, while at the green sites they are fourfold coordinated. The energy required to incorporate In at the red sites is more than 0.87 eV higher than at the green position.

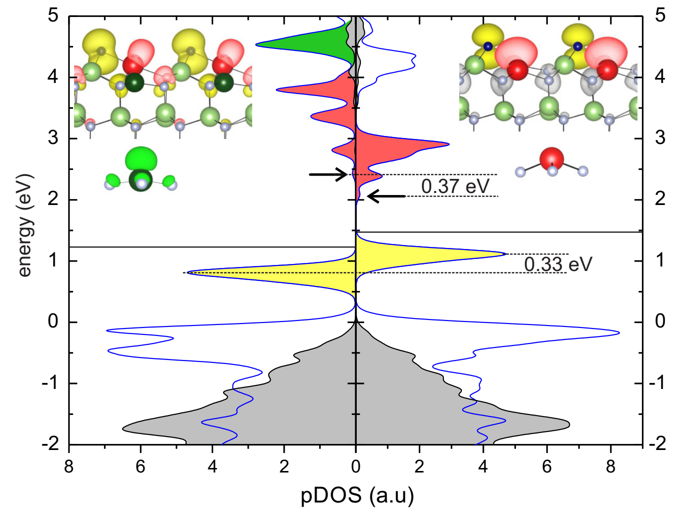

FIG. 3. On-site projected density of states (pDOS) of a 2×2 N adatom (0001) GaN surface with 25% InN at the topmost surface layer. (a) and (b) The In atom sits at a fourfold/triply coordinated site, respectively. The blue curves indicate the pDOS on the N adatom and on the first surface layer atoms. The gray shaded area denotes the pDOS from the fourth surface layer and the yellow shaded area the highest occupied surface state. The arrows indicate the onset of the lowest unoccupied surface states and the horizontal solid lines the position of the highest occupied states. (Insets) Yellow, red, and green colored density plots indicate the partial charge density of the states in the energy range shaded in yellow, red, and green in the pDOS, respectively. (Insets bottom) Schematic representation of the tetrahedra formed by the triply coordinated metal atoms and the three N atoms bound to them. The red/green isocontour surface shows the corresponding dangling bond state. Dark/light small balls denote the N adatom/atoms, respectively. Red/green balls are the In/Ga atoms, respectively. The dark green in the left inset denote the triply coordinated Ga atom.

under N-rich conditions, In prefers surface sites that according to our present understanding should be highly unfavorable.

The representative model sketched in Fig. 2 allows us to visualize all the identified low-energy structures. It consists of a metal-polar $(2\sqrt{3} \times 2\sqrt{3})\text{R}30^\circ$ surface with three triply coordinated N adatoms on top. This structure obeys the ECR by construction, independent of the specific distribution of the In and Ga atoms in the metal layer. The blue and green colors mark fourfold coordinated and the red one threefold coordinated metal atoms. To account for the elastic repulsion between two neighboring In atoms, the four-fold coordinated sites are split into two colors: considering that an In atom occupies a blue site, it should be energetically unfavorable for another In atom to occupy a neighboring green site. Starting from an In-free 2×2 N adatom surface, we systematically replace Ga by In atoms. In each step, we compute the energy for a single substitution on all symmetry inequivalent sites. To proceed to more In, we then keep the lowest energy configuration found at this stage, and compute the substitution energies when adding one more In atom. The corresponding Ga-In exchange energies, relative to the substitution of a single In, are plotted in Fig. 2 and show a clear gap in the order of an eV between the three- and fourfold coordinated sites in favor of the latter. Surprisingly, the actually observed energetic trends defy our previous understanding that the surface tries to minimize the number of weak In-N bonds. Rather, In has a strong tendency to go onto a four-fold coordinated site leaving a Ga atom on the threefold site. Furthermore, bringing two In atoms onto nearest neighbor sites (blue and green) costs a small energy penalty (50–150 meV per pair). As the total In concentration increases, the number of such pairs inevitably grows when the In is put outside the sublattice depicted in blue, creating an increasing gap between the next low-energy site (blue) and the less favorable ones (green).

The trends in the computed chemical potential for the various sites immediately explains the observed experimental limitations in achieving higher In concentrations as well as chemical ordering. Substituting In on only the blue sites leaves the chemical potential essentially flat, i.e., adding one, two, or three In atoms costs essentially the same energy. However, adding a fourth In atom and thus increasing the In concentration from 1/4 to 1/3 increases the In potential by ≈0.3 eV. To realize this increase in the In chemical potential in our MBE would require to raise the In flux by a factor of ≈5. Such a huge increase in the In flux would eventually switch the growth conditions to In-rich, which will either stabilize two MLs of In on the surface or flood the surface with In, resulting in In droplets and poor growth morphology. The challenge to realize such a huge increase in the chemical potential becomes even more evident when comparing this value with the heat of formation of InN (0.2 eV) which corresponds

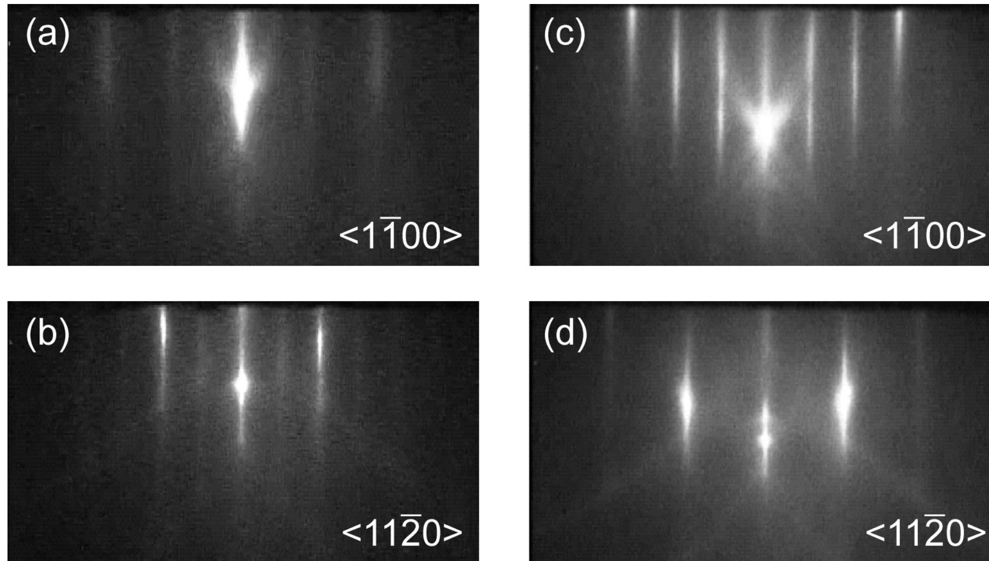

FIG. 4. *In situ* RHEED pattern after deposition of (a) and (b) GaN, as well as (c) and (d) InN along the $\langle 1\bar{1}00\rangle$ and the $\langle 11\bar{2}0\rangle$ azimuth, respectively.

to the maximum interval the potential can have when in thermodynamic equilibrium with InN.

The question remains which mechanism stabilizes a structure that violates the established principles. In order to address this question, we compare the electronic density of states (DOS) of a surface where the In atom occupies one of the low-energy fourfold coordinated (blue) sites with that of the configuration where the In atom is sitting on one of the triply coordinated (red) sites (see Fig. 3). The latter configuration should be the preferred configuration, following the established chemical bond-strength principle. As can be seen in the DOS, the large energy gain of the fourfold coordinated site is a direct consequence of a sizable downward-shift of a doubly occupied surface band (marked by the yellow color). An inspection of the corresponding wave function reveals that this doubly occupied surface band for both structures is related to the dangling bond state of the neighboring surface N adatom (yellow isocontour surface in Fig. 3).

This result may come as a surprise, since the N adatom has in both structures the same three-fold coordination. Inspecting the unoccupied states reveals the underlying mechanism: As shown in Fig. 3 the unoccupied orbitals of the energetically preferred structure with the fourfold coordinated In atom are shifted upwards. While the unoccupied states have no direct impact on the energetics and thus the thermodynamic stability of the surface, according to the bond orbital picture an upward shift of the antibonding orbital is accompanied by a downshift of the occupied bonding orbital, which effectively reduces the energy of the system. The downshift of the occupied orbital though cannot be observed directly, because it hybridizes with the valence-band manifold below the band gap.

Let us now consider the triply coordinated cation. The triply coordinated cation at the free surface (red color in Fig. 3) can relax by shifting its position along the surface normal. In case of Ga this flexibility allows the cation dangling bond to rehybridize from the bulklike sp^3 dangling bond configurations to a more p-like configuration (raising the energy as seen in Fig. 3) while the back bonds rehybridize from sp^3 to a planar sp^2 configuration. The sp^2 configuration lowers the bond energy with the N atoms and leads to an inward displacement of the triply coordinated cation. While a Ga atom, which fits to the underlying lattice, gains energy through this energetically favorable rehybridization, this is not the case for an In. The inward displacement of the atom in this case would be inhibited by the too large atomic radius of the In atom. The necessary strain energy exceeds the gain due to rehybridization and thus causes a large elastic frustration. We call this new mechanism, which causes the technologically well-known stoichiometric limitations in (In,Ga)N alloys, *elastically frustrated rehybridization*.

Comparing our experimental TEM images against image simulations based on the above identified $(2\sqrt{3}\times 2\sqrt{3})\mathrm{R}30^\circ$ configuration and considering a residual chemical disorder,[1] we find excellent agreement on the near atomic level between simulation and experiment [see Figs. 1(c) and 1(d) for the $\langle 1\bar{1}00\rangle$ and the $\langle 11\bar{2}0\rangle$ zone axis, respectively]. Even fine details such as the slightly increased intensity below the darker intensity spots (corresponding to the In-rich atomic columns) in the $\langle 1\bar{1}00\rangle$ projection can be identified in the experiment. However, an unequivocal identification of the atomic configuration solely by contrast analyses would require larger areas of ordered patches (see supplemental material). To distinguish between the two structures, we determined the In concentration in the ML by a lattice parameter analysis which is discussed in the supplemental material. This analysis yields an In concentration of 25%, allowing to rule out the $(\sqrt{3}\times\sqrt{3})\mathrm{R}30^\circ$ structure in perfect agreement with the *ab initio* predictions.

To further verify that the *ab initio* predicted $(2\sqrt{3}\times 2\sqrt{3})\mathrm{R}30^\circ$ surface with 25% In content is indeed the source

[1] 10% of the In atoms were randomly distributed.

of the observed chemical ordering and the compositional limitations we investigated the respective reconstructions during growth by RHEED. At the end of the GaN barrier growth, the RHEED exhibits a 2×2 surface reconstruction, as displayed in Figs. 4(a) and 4(b) for the $\langle 1\bar{1}00 \rangle$ and the $\langle 11\bar{2}0 \rangle$ azimuth, respectively. This reconstruction is the expected one for N-rich conditions of GaN and agrees with surface calculations of Northrup *et al.* [32]. Subsequent deposition of InN leads to a $3\times$ periodicity along the $\langle 1\bar{1}00 \rangle$ azimuth, while a $1\times$ periodicity persists along the $\langle 11\bar{2}0 \rangle$ azimuth, as shown in Figs. 4(c) and 4(d), respectively. These observations are consistent with those described in Ref. [25], which the authors interpreted as a $(\sqrt{3} \times \sqrt{3})$R30° reconstruction. However, the differences between a $(2\sqrt{3} \times 2\sqrt{3})$R30° and a $(\sqrt{3} \times \sqrt{3})$R30° N-adatom reconstruction in RHEED are negligible (see supplemental material). A previous *in situ* RHEED study estimated that the $3\times$ streak intensity along the $\langle 1\bar{1}00 \rangle$ azimuth maximizes for a nominal In coverage of around 0.33 [21]. Since in this estimate desorption and decomposition have not been included, which both decrease the actual In content, the lower In content with 25% predicted by our *ab initio* study and TEM analyses appears to be consistent. Our RHEED data show the $3\times$ periodicity along the $\langle 1\bar{1}00 \rangle$ azimuth to be stable for temperature as high as 650 °C (see Ref. [27]). This is a remarkably high temperature when compared against typical growth temperatures for (In,Ga)N alloys with a high In content [6]. Further InN deposition causes a reduction of the 1×3 RHEED reflex intensity. We trace this back to the fact that once the In content in the ML reaches 25%, further In incorporation is inhibited but instead accumulated on the surface. The same argument also explains our experimental observation that the thickness of the (In,Ga)N is limited to a single ML.

In summary, by combining TEM, RHEED, and DFT calculations we have demonstrated that the growth of nominal InN MLs on GaN (0001) by MBE under slightly N-rich growth conditions leads to ordered MLs with a mean In content of 25%, irrespective of the amount of In provided to the surface. The severe limitation of the In concentration is explained by a novel mechanism, elastically frustrated rehybridization, which prevents In atoms from occupying low-coordinated surface sites. The observed preference of In for fourfold coordinated surface sites reveals not only a novel mechanism, but has direct consequences for the growth of these technologically highly relevant films: its high thermodynamic stability limits the maximum In concentration to 25% as well as the thickness to a single ML when switching off the Ga flux. Our findings are the first example of a surface induced ordered InGaN quantum well in the III nitrides and reveal fundamental limitations for extending the compositional range for this material system via digital alloying. The observed mechanism may also open the route to growing purposefully ordered ML alloys in (In,Ga)N/GaN and possibly other alloy systems, which substantially reduces compositional disorder. Also, it may help to identify possible strategies that prevent this mechanism thus allowing to overcome this stoichiometric limit and to achieve higher In concentrations.

ACKNOWLEDGMENTS

We thank R. Calarco and C. Skierbiszewski for MBE advice and T. Markurt for TEM imaging. Funding of this work by the European Union's Horizon 2020 research and innovation program (Marie Skłodowska-Curie Actions) under Grant Agreement "SPRInG" No. 642574 and FP7-NMP-2013-SMALL-7 program under Grant Agreement No. 604416 (DEEPEN) is gratefully acknowledged. X.Q.W. acknowledges support from the National Key Research and Development Program of China (No. 2016YFB0400100), Science Challenge Project (No. TZ2016003-2), the Sino-German Center for Science Promotion, NSFC and DFG (GZ1309), and NSAF (No. U1630109).

L.L. and T.S. contributed equally to this work.

[1] H. Kroemer, Proc. IEEE **51**, 1782 (1963).
[2] R. Dingle, W. Wiegmann, and C. H. Henry, Phys. Rev. Lett. **33**, 827 (1974).
[3] R. Dupuis and P. D. Dapkus, Appl. Phys. Lett. **31**, 466 (1977).
[4] W. C. Yang, C. H. Wu, Y. T. Tseng, S. Y. Chiu, and K. Y. Cheng, J. Appl. Phys. **117**, 015306 (2015).
[5] G. R. Mutta, P. Ruterana, J. L. Doualan, M. P. Chauvat, F. Ivaldi, S. Kret, N. A. K. Kaufmann, A. Dussaigne, D. Martin, and N. Grandjean, Phys. Status Solidi B **248**, 1187 (2011).
[6] M. Siekacz, M. Sawicka, H. Turski, G. Cywiński, A. Khachapuridze, P. Perlin, T. Suski, M. Boćkowski, J. Smalc-Koziorowska, M. Kryśko, R. Kudrawiec, M. Syperek, J. Misiewicz, Z. Wasilewski, S. Porowski, and C. Skierbiszewski, J. Appl. Phys. **110**, 063110 (2011).
[7] G. B. Stringfellow, J. Cryst. Growth **27**, 21 (1974).
[8] D. M. Wood and A. Zunger, Phys. Rev. Lett. **61**, 1501 (1988).
[9] A. Zunger and S. Mahajan, in *Handbook on Semiconductors*, edited by S. Mahajan (Elsevier, Amsterdam, 1994), Vol. 3b, p. 1399.
[10] J. E. Bernard, S. Froyen, and A. Zunger, Phys. Rev. B **44**, 11178 (1991).
[11] J. Tersoff, Phys. Rev. Lett. **74**, 434 (1995).
[12] G. Stringfellow, J. Appl. Phys. **43**, 3455 (1972).
[13] M. Quillec, H. Launois, and M. C. Joncour, J. Vac. Sci. Technol. B **1**, 238 (1983).
[14] M. J. Jou, Y. T. Cherng, H. R. Jen, and G. B. Stringfellow, Appl. Phys. Lett. **52**, 549 (1988).
[15] R. M. Cohen, M. J. Cherng, R. E. Benner, and G. B. Stringfellow, J. Appl. Phys. **57**, 4817 (1985).
[16] S. Yu. Karpov, MRS Internet J. Nitride Semicond. Res. **3**, e16 (1998).
[17] S. B. Zhang and S. H. Wei, Phys. Rev. Lett. **86**, 1789 (2001).
[18] M. Albrecht, H. Abu-Farsakh, T. Remmele, I. Hausler, L. Geelhaar, H. Riechert, R. Fornari, and J. Neugebauer, Phys. Rev. Lett. **99**, 206103 (2007).
[19] I. Gorczyca, T. Suski, N. E. Christensen, and A. Svane, Cryst. Growth Des. **12**, 3521 (2012).
[20] S. Chichibu, T. Azuhata, T. Sota, and S. Nakamura, Appl. Phys. Lett. **70**, 2822 (1997).
[21] C. Chèze, F. Feix, M. Anikeeva, T. Schulz, M. Albrecht, H. Riechert, O. Brandt, and R. Calarco, Appl. Phys. Lett. **110**, 072104 (2017).

[22] C. Chèze, M. Siekacz, F. Isa, B. Jenichen, F. Feix, J. Buller, T. Schulz, M. Albrecht, C. Skierbiszewski, R. Calarco, and H. Riechert, J. Appl. Phys. **120**, 125307 (2016).
[23] X. Wang, S. Liu, N. Ma, L. Feng, G. Chen, F. Xu, N. Tang, S. Huang, K. J. Chen, S. Zhou, and B. Shen, Appl. Phys. Express **5**, 015502 (2012).
[24] S. T. Liu, X. Q. Wang, G. Chen, Y. W. Zhang, L. Feng, C. C. Huang, F. J. Xu, N. Tang, L. W. Sang, M. Sumiya, and B. Shen, J. Appl. Phys. **110**, 113514 (2011).
[25] H. J. Chen, R. M. Feenstra, J. E. Northrup, T. Zywietz, J. Neugebauer, and D. W. Greve, J. Vac. Sci. Technol. B **18**, 2284 (2000).
[26] S. Lee, C. Freysoldt, and J. Neugebauer, Phys. Rev. B **90**, 245301 (2014).
[27] See Supplemental Material at http://link.aps.org/supplemental/10.1103/PhysRevMaterials.2.011601 for more details on the methodology, bulk order-disorder transition temperatures and RHEED simulations.
[28] W. A. Harrison, J. Vac. Sci. Technol. **16**, 1492 (1979).
[29] M. Himmerlich, L. Lymperakis, R. Gutt, P. Lorenz, J. Neugebauer, and S. Krischok, Phys. Rev. B **88**, 125304 (2013).
[30] J. E. Northrup, L. T. Romano, and J. Neugebauer, Appl. Phys. Lett. **74**, 2319 (1999).
[31] A. I. Duff, L. Lymperakis, and J. Neugebauer, Phys. Rev. B **89**, 085307 (2014).
[32] J. E. Northrup, J. Neugebauer, R. M. Feenstra, and A. R. Smith, Phys. Rev. B **61**, 9932 (2000).